

# Modern Spin-Wave Nonlinear Dynamics

Flavio M. de Aguiar, Antonio Azevedo and Sergio M. Rezende

*Departamento de Física, Universidade Federal de Pernambuco*

*50732-970 Recife, Brasil*

Received October 15, 1992

A review of our own experimental and theoretical work on high-power ferromagnetic resonance phenomena is given. Four topics are examined, namely, (1) the onset of spin-wave instabilities, (2) the onset of spin-wave auto-oscillations, (3) higher-order bifurcations as transitions to chaos and (4) the control of spin-wave chaos.

## I. Introduction

Universality has greatly increased the interest in dissipative dynamical systems during the last decade. In particular, spin waves driven by strong microwave ( $1 - 10$  GHz) fields in magnetic materials have proven very attractive.

The birth of high-power ferromagnetic resonance may be traced back to the pioneering experiments of Bloembergen, Damon and Wang in the early 50s<sup>1</sup>. They have observed a premature saturation of the main resonance absorption and the appearance of a subsidiary absorption when the microwave power exceeded certain threshold levels. A theory by Suhl<sup>2</sup>, introduced a few years later, is still the basis for explaining the phenomena. Suhl's theory relied upon the parametric excitation of spin-wave pairs via two- and one-photon decay processes. Soon after, it was demonstrated<sup>3</sup> that spin waves could also be parametrically pumped by a microwave field parallel to the dc magnetic field,  $\vec{h} // \vec{H}_0$ . This was called the parallel pumping process to distinguish from the standard magnetic resonance configuration,  $\vec{h} \perp \vec{H}_0$ . Here, these three processes are generically said to occur when the microwave field is increased beyond the Suhl instability (SI) threshold,  $h_c$ .

Suhl was also the first to realize that the phenomena bore resemblance to fluid dynamics. Spin-wave experiments were then observed to exhibit a remarkable effect still in the early 60s. At a subsequent threshold  $h'_c > h_c$ , a low-frequency ( $10$  kHz -  $1$  MHz) oscillation was observed as a modulation in the power absorbed by the sample<sup>4</sup>. This oscillatory instability, or auto-oscillation, was firstly attributed to the excitation of standing spin waves in the sample<sup>5</sup>, but this model was never completely understood<sup>6</sup>. On the other hand, several Soviet authors<sup>7</sup> had shown that the auto-oscillation could result from the nonlinear dynamics of spin waves in an infinite medium but the quantitative results of their model were also unsatisfactory.

Spin-wave experiments have enjoyed a revival of interest in the 80s since it was predicted<sup>8</sup> and experimen-

tally observed<sup>9,10</sup> that ferrimagnets exhibit the period-doubling route to chaos at higher power levels ( $h > h'_c$ ). A large number of theoretical and experimental results followed those findings and definitely placed the spin-wave among the most interesting nonlinear dissipative dynamical systems to be investigated<sup>11</sup>.

In all three parametric processes, the SI threshold  $h_c$  is determined by the rate at which energy must be pumped into the spin-wave mode to overcome the power dissipated to the lattice. Since both the coupling to the microwave field and the relaxation rate depend on the wave vector  $\vec{k}$ , there is a certain mode for which  $h_c$  is a minimum. Increasing the microwave field beyond this value results in the excitation of many other modes and complexity increases accordingly. As far as theory is concerned, we sidestep this problem by considering the dynamics of only two modes.

In the first part of this paper we review the experimental situation of nonlinear phenomena associated with spin-wave instabilities, including the intriguing step-like behavior of transients prior to auto-oscillation<sup>12</sup> and the control of spin-wave chaos<sup>13</sup> recently observed. The ongoing discussion regarding the nature of the excited modes is considered in the second part, where we point out the successes and failures of the two-mode model.

## II. Spin-wave experiments

The results presented here were obtained with yttrium-iron-garnet (YIG) spheres and films at room temperature, using the experimental set-up shown schematically in Fig.1. The sample is held at the center of a critically coupled TE<sub>102</sub> microwave cavity with  $Q \simeq 2000$ , placed between the poles of an electromagnet that provides the static field  $\vec{H}_0$ . The cavity can be oriented so that the microwave magnetic field  $\vec{h}$  is either parallel or perpendicular (subsidiary resonance) to  $\vec{H}_0$ . The microwave radiation is generated by a X-band backward-wave oscillator (BWO) and amplified to 2.0 Watt by a traveling-wave tube (TWT). The BWO frequency is stabilized by an external crystal oscillator and

manually adjusted to the center of the cavity resonance. The radiation power is then controlled with a variable precision attenuator and directed by a circulator to the resonant cavity, where it drives spin waves in the sample. The reflected microwave signal is detected with a sensitive Schottky-barrier diode at the output port of the circulator and recorded in a digital storage oscilloscope or observed with a spectrum analyzer. In order to avoid sample heating the microwave radiation is pulsed (duration 100  $\mu\text{sec}$  at 100 pulses/sec) with a PIN modulator placed before the TWT amplifier. This causes no difficulty for recording the steady-state regime of the sample response because the transient time is normally much shorter than the pulse duration.

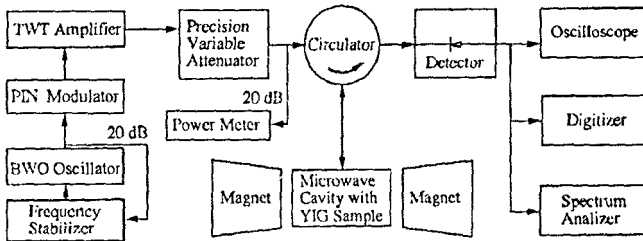


Figure 1: Schematic diagram of the microwave system used to excite spin-wave instabilities.

### 11.1 The onset of spin-wave instabilities and auto-oscillations

At low-power levels the pulse reflected from the cavity has essentially the same shape as the incoming microwave pulse (Fig.2(a)). As the power is increased, an abrupt change occurs at the end of the reflected pulse, corresponding to the build-up of a spin-wave mode after a delay time  $\tau$ . Actually, the build-up time is infinite at  $h = h_c$ , and decreases rapidly with increasing field, according to a scaling law  $\tau \sim (h/h_c - 1)^{-\gamma}$ . Fig.2(b) shows this stage of parametric excitation in a 1 mm diameter YIG sphere with subsidiary-resonance pumping for  $h/h_c \simeq 1.05$ . At larger excitation, another spin-wave mode builds up, as shown in Fig.2(c) for  $h/h_c \simeq 1.12$ . As  $h$  increases further, no other mode appears before the onset of auto-oscillation, shown in Fig.2(d) for  $h_c'/h_c \simeq 1.7$ . Only recently<sup>12</sup> we have observed the step-like behavior shown in Fig.2, which sheds light on the unsolved problem regarding the number of modes excited above the SI threshold, as we will discuss later. However, we stress that the overall situation is rather complex. In some cases only one step appears before the onset of auto-oscillation and in other situations up to three steps have been observed.

The gross features of the spin-wave instabilities driven in subsidiary resonance are similar to those in parallel pumping. Fig.3(b) shows the phase boundaries for spin wave excitation and auto-oscillation measured

in the same 1 mm YIG sphere of Fig.3(a) with  $\vec{H}_0$  along the [110] axis and microwave frequency 8.87 GHz. Instead of a sharp minimum, the "butterfly curve" for subsidiary resonance has a broad minimum and three characteristic regions in field  $H_0$ . For  $H_0 < H_c \simeq 1580$  Oe the modes with lowest threshold are plane waves with  $k > 0$  propagating at an angle  $\theta_k = \pi/4$  with  $\vec{H}_0$  (or  $\theta_k \simeq 35^\circ$  depending on the effect of the relaxation rate). For  $H_c < H_0 < H_c' = 2190$  Oe the modes with minimum threshold are magnetostatic waves with  $k \approx 0$ . For  $H_0 > H_c'$  the threshold rises sharply with  $H_0$  as  $\theta_k \rightarrow 0$ . Since in the various field regions the modes excited have different nonlinear coupling parameters, a variety of bifurcations leading to self-oscillations can be observed at different field values, as indicated by the boundary lines in Fig.3(b). In the parallel-pumping case, modes with  $\theta_k = \pi/2$  and wave number  $k = [(H_c - H_0)/D]^{1/2}$  are excited at the minimum SI threshold  $h_c = 2\omega_p\gamma_k/\gamma\omega_M$ . Here,  $D$  is the exchange stiffness ( $D = 5.4 \times 10^{-9}$  Oe.cm<sup>2</sup> for YIG),  $\omega_p = 2\pi f_p$  is the pumping frequency,  $\gamma = g\mu_B/h$  is the gyromagnetic ratio,  $\omega_M = \gamma 4\pi M$ ,  $M$  is the saturation magnetization ( $4\pi M = 1750$  Oe for YIG at 300 K) and  $\gamma_k$  is the phenomenological relaxation rate. Notice that this is valid for  $H_0 < H_c$  (Fig.3(a)) and in this field range the parallel pumping process enables one to measure  $\gamma_k$  as a function of  $k$ .

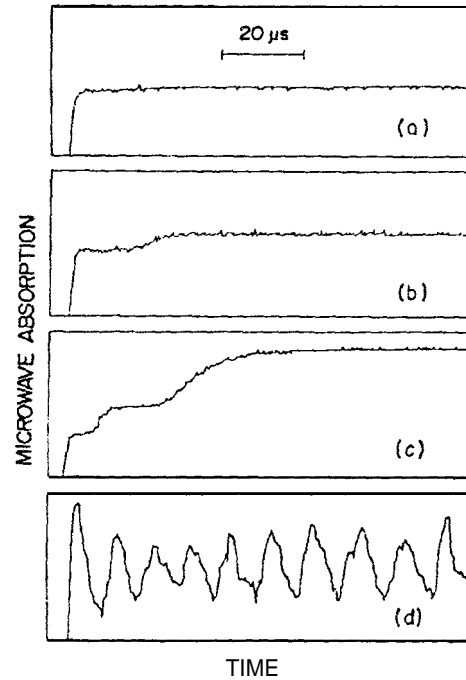


Figure 2: Storage oscilloscope recordings of the reflected microwave pulse obtained with subsidiary resonance in a 1 mm YIG sphere, with  $H_0 = 2.0$  kOe along [111] and  $f_p = 8.2$  GHz. The various traces correspond to microwave fields (a)  $R = h/h_c \simeq 0.05$ , (b) 1.05, (c) 1.12 and (d) 1.7.

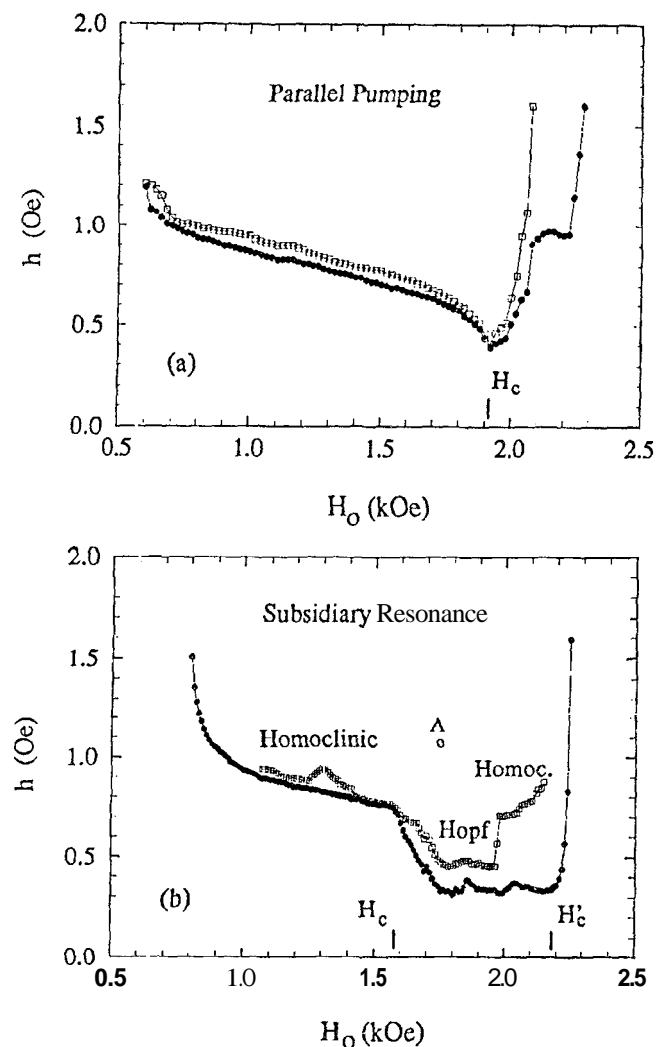


Figure 3: TI reshold microwave fields  $h$ , ( $\bullet$ ) and  $h'_c$  ( $\square$ ) versus dc field  $H_0$  in a 1mm YIG sphere for (a) parallel pumping at  $f_p = 12.0$  GHz,  $\vec{H}_0$  aloiig [111] and (b) subsidiary resonance at  $f_p = 8.87$ GHz,  $H_0$  aloiig [110].

The auto-oscillations that appear at  $h > h'_c$  have shape and frequency which depend on the pumping level, dc field value, crystal axis orientation with respect to  $\vec{H}_0$  and a so on sample dimensions, surface polishing and temperature. Fig.4(a) shows the oscilloscope traces of the self-oscillations with increasing pumping in the parallel pumping configuration at  $H_0 = 1570$  Oe,  $f_p = 9.5$  GHz. The oscillations appear at a field  $h'_c$  just above the SI threshold with a finite frequency  $f_0 \approx 220$  kHz and vanishing amplitude  $A$ . As  $h$  increases the amplitude increases smoothly while the frequency stays constant. The detailed data reveal that  $A$  varies with the reduced driving field  $r = h/h'_c - 1$  in the critica region as  $A \sim r^\beta$ , where  $\beta = 0.5$ . This is typical of a Hopf bifurcation and is analogous to a second-order phase transition<sup>14-17</sup>.

Quite different behavior is shown in Fig.4(b) by the oscilloscope traces obtained in subsidiary resonance

pumping with  $\vec{H}_0$  aloiig the [110] axis of the YIG sphere, as in Fig.3(b), with  $H_0 = 1950$  Oe,  $f_p = 8.87$  GHz. In this case the auto-oscillation sets in with finite amplitude and vanishing frequency, in analogy with a first-order phase transition and in marked contrast with the scenario of Fig.4(a). This has been identified as a homoclinic bifurcation<sup>16,17</sup>.

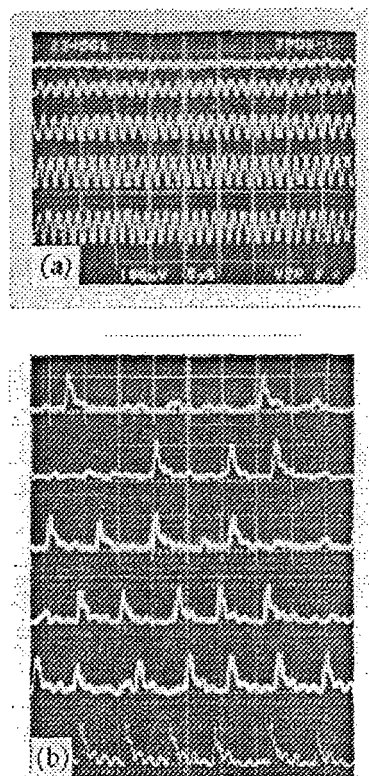


Figure 4: Oscilloscope traces showing the behavior of the auto-oscillation with increasing microwave field. (a) Hopf bifurcation observed with parallel pumping in a YIG sphere,  $H_0 = 1570$  Oe along [111],  $f_p = 9.5$  GHz, and  $\mathcal{E} = 1.224, 1.255, 1.293, 1.321$  and  $1.342$  from top to bottom. (b) Homoclinic bifurcation observed in subsidiary resonance with the same sphere,  $H_0 = 1950$  Oe along [110] and  $R = 1.862, 1.872, 1.883, 1.894, 1.905$  and  $1.916$  from top to bottom [Ref.17].

In Fig.5 we experimentally characterize the onset of auto-oscillation by measuring the ratio of the fundamental harmonic to the relaxation rate,  $f_0/\gamma_k$ , for YIG spheres (Fig.5(a)) and films (Fig.5(b)) with different dimensions. The results unequivocally show that the sample dimension plays a role in determining the auto-oscillation frequency for the  $k$  values accessible in parallel-pumping experiments. The higher the dimension, the lower the ratio  $f_0/\gamma_k$ .

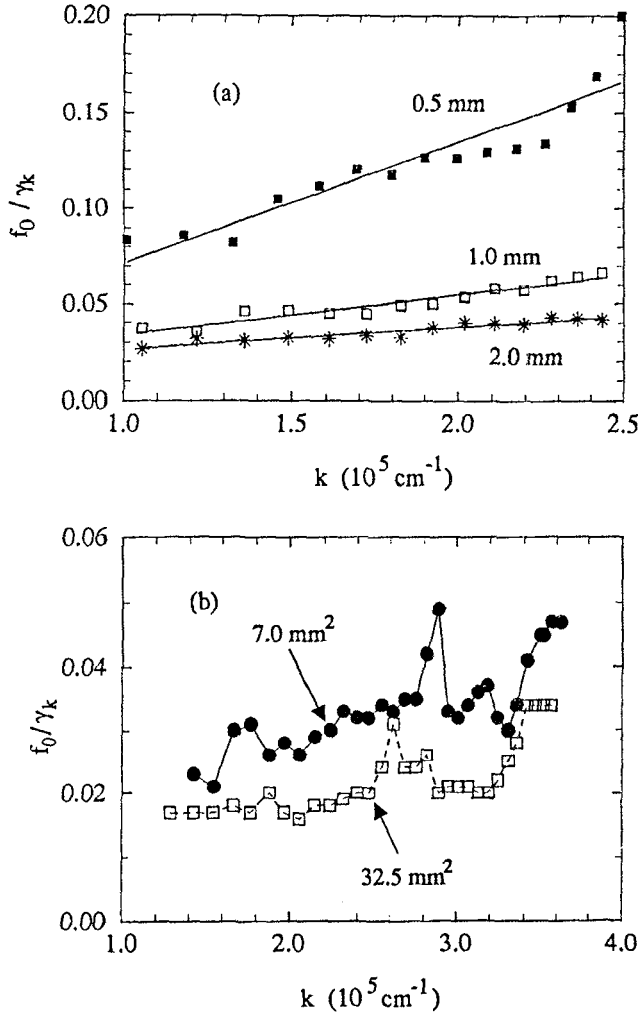


Figure 5: Ratio of the auto-oscillation frequency  $f_0$  to the relaxation rate  $\gamma_k$  at threshold, as a function of  $k$  for YIG spheres (a) and films (b) with different dimensions, observed in parallel pumping experiments. The solid lines in (a) are linear fits and in (b) are guides to the eyes.

## II.2 Higher-order bifurcations

The nonlinear signature of the spin-wave auto-oscillation is clearly demonstrated at higher power levels ( $h > h_c$ ). Universal behavior such as relaxation oscillations, period multiplication, quasiperiodicity, intermittency, chaos and chaotic transitions has been reported by many authors<sup>11</sup>, in all three parametric processes described above. Here we give a few examples of this rich dynamical behavior of spin waves, observed in the perpendicular pumping of the subsidiary resonance in the YIG sphere for which the threshold fields  $h_c(H_0)$  and  $h'_c(H_0)$  are given in Fig.3(b).

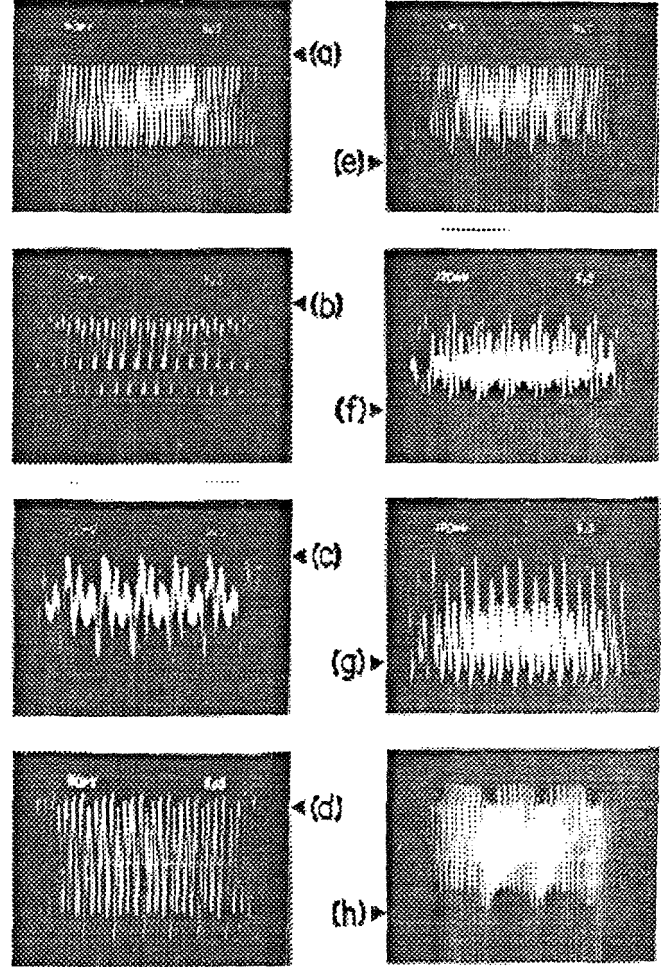


Figure 6: Oscilloscope traces showing (a) period-1, (b) period-2, (c) period-3, (d) period-4, (e) period-5, (f) period-5, but with different pattern from (e), (g) period-6 and (h) quasiperiodic oscillations observed in subsidiary-resonance experiments in a YIG sphere for different combinations of crystal orientation,  $H_0$  and  $R$  [Ref.18].

Let us define  $R \equiv h/h_c$  as the control parameter. In general, the auto-oscillation amplitude and frequency increase with  $R$ . For certain values of  $H_0$  and crystal directions we may observe the appearance of even or odd subharmonics or unlocked (quasiperiodic) oscillatory regimes, as depicted in Fig.6 [18]. Ordered transitions to chaos may also be observed either with fixed  $H_0$  and varying  $h$  or with fixed  $h$  and varying  $H_0$ . The period-doubling route to chaos is nicely seen in Fig.7 for  $H_0 = 1950 \text{ Oe}$  and  $2.12 \leq R \leq 2.54$ <sup>19</sup>. Chaotic behavior in spin-wave experiments has been characterized as low-dimensional chaos<sup>19a,19b</sup>, indicating that few modes participate in the spin-wave nonlinear dynamics, even in the regime of hyperchaos<sup>19c</sup>.

Another interesting scenario is shown in Fig.8 for  $h = 0.46 \text{ Oe}$  and the sample oriented with the [111] direction along  $\vec{H}_0$ . In this case, an intermittent transition to chaos is seen with decreasing  $H_0$ , with val-

ues 1900, 1868, 1860, 1850 and 1840 Oe, from bottom to top, respectively. This scenario has been investigated in the light of the theory of crisis in dissipative systems<sup>20,21,22</sup> and quantitative measurements of the distributions of the laminar periods duration and the dependence of the mean time on the control parameter are underway.

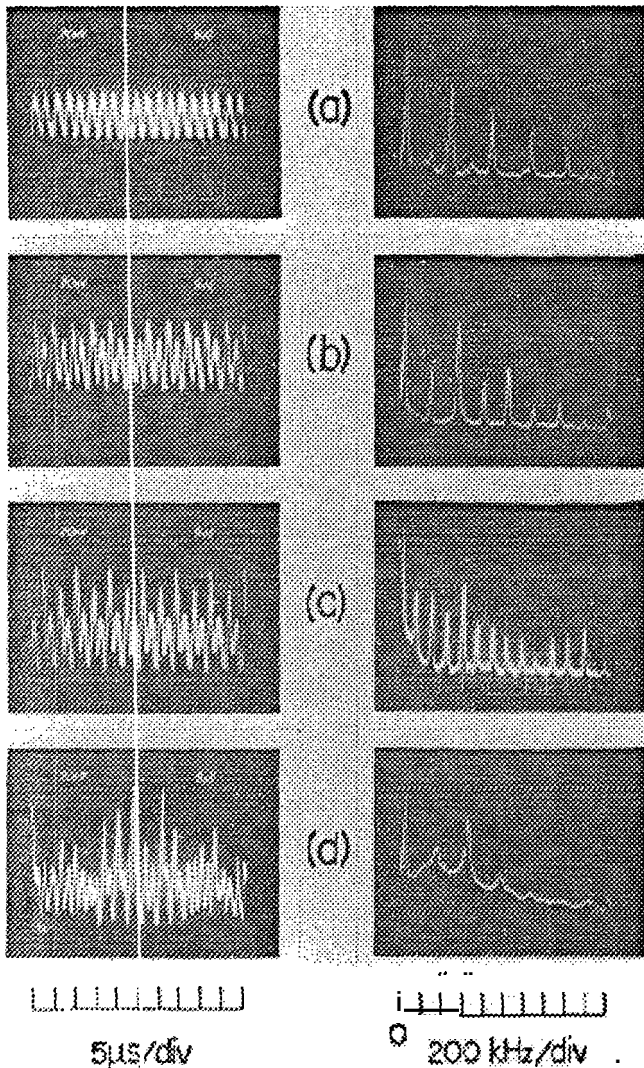


Figure 7: Oscilloscope traces showing (a) period-1, (b) period-2, (c) period-4 and (d) chaotic oscillations and corresponding power spectra observed in subsidiary-resonance experiments in a YIG sphere at  $R = 2.12, 2.17, 2.29$  and  $2.54$ , respectively [Ref.19].

### 11.3 Controlling spin-wave chaos

The feasibility of controlling chaos by a small time-dependent perturbation of the biasing magnetic field applied to the sample was recently demonstrated<sup>13</sup>. The method is based on the fact that a chaotic attractor usually has embedded within it an infinite number of unstable periodic orbits. By applying a small time-dependent modulation to a conveniently chosen parameter one can stabilize some of these orbits to achieve

control of the chaotic state, as predicted by Ott, Grebogi and Yorke<sup>23</sup>.

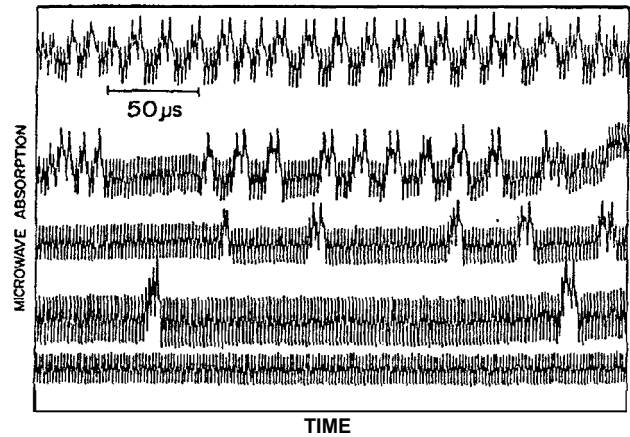


Figure 8: Intermittent transition to chaos observed in subsidiary-resonance experiments in a YIG sphere with  $h = 0.46$  Oe and  $\vec{H}_0$  along [111].  $H_0 = 1900, 1868, 1860$  and  $1810$  Oe from bottom to top, respectively [Refs.20,21].

The control of spin-wave chaos was achieved in the subsidiary resonance configuration with the 1 mm YIG sphere with the [110] direction aligned with  $\vec{H}_0$ . We have added inside the microwave cavity a loop of diameter 1.5 cm made with a 0.5 mm copper wire to allow the modulation of the static magnetic field,  $H = H_0 + \delta H \cos(2\pi f_m t)$ , over a broad frequency range ( $0 < f_m < 10$  MHz), typically with  $\delta H/H_0 \sim 10^{-4}$ . The results presented here were observed after the system has been driven to a fully chaotic regime with  $h = 1.1$  Oe and  $H_0 = 1750$  Oe, represented by the point A in Fig.3(b). Fig.9(a) shows the power spectrum of a chaotic auto-oscillation for  $\delta H = 0$ , displaying a characteristic broadband feature. By increasing  $\delta H$ , the spectrum becomes progressively cleaner, with sharp lines characteristic of a periodic signal. Fig.9(b) shows the result for  $\delta H = 0.435$  Oe and  $f_m = 1480$  kHz. The spectrum in this case corresponds to a quasiperiodic signal with fundamental frequencies  $f_0 = 740$  kHz and  $f_1 = 1975$  kHz, and a subharmonic component at  $f_0/2$ . In Fig.10 we show the variation of the critical amplitude  $\delta H^*$  necessary to control chaos with the modulation frequency  $f_m$  measured at point A in Fig.3(b). Notice that  $\delta H^*$  has minima at values commensurate with the fundamental frequency  $f_0$ , i.e.,  $f_0/f_m = p/q$ , where  $p$  and  $q$  are integers. In addition, for the  $f_m$  range shown in Fig.10, the minima are strikingly ordered according to the devil's staircase, i.e., the minimum detected between  $p/q$  and  $p'/q'$  is characterized by the ratio  $(p + p')/(q + q')$ .

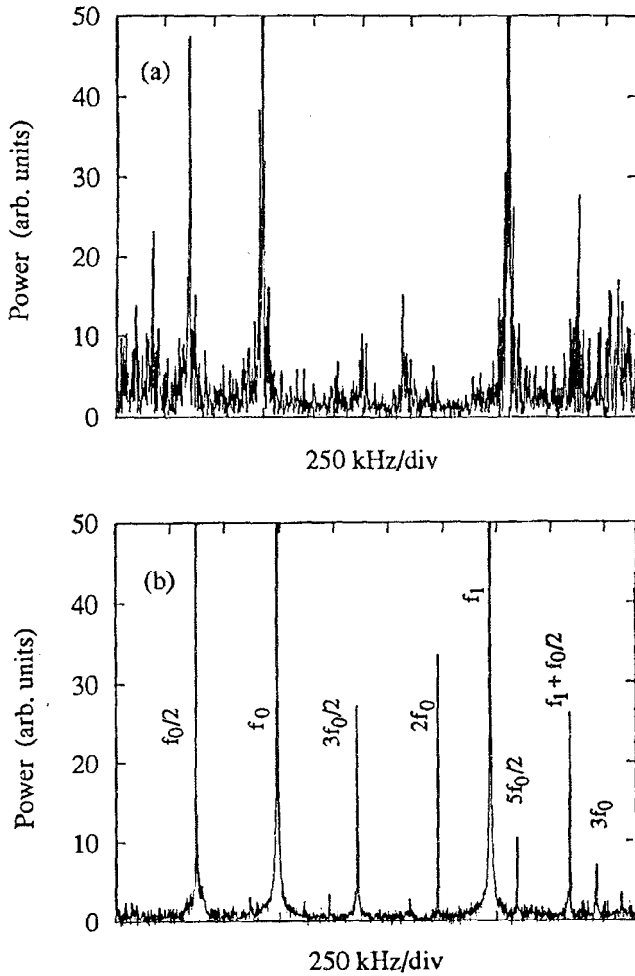


Figure 9: Power spectra of auto-oscillations observed at point *A* of Fig.3b for different values of the amplitude  $\delta H$  of the field modulation. (a) Chaos for  $\delta H = 0$ . (b) Chaos under control with  $611 = 0.435$  Oe and  $f_m = 1480$  kHz. [Ref.13].

### III. Theoretical model

The basic physical ideas developed by Suhl in the late 50s<sup>2</sup> regarding the theory of high-power ferromagnetic resonance retain their validity nowadays. However, despite the recent progress in the understanding of spin-wave nonlinear dynamics, a definitive correspondence between experiment and theory remains elusive, even in the pre-diaotic regime<sup>12</sup>. In this section we give a brief review of the two-mode-model (TMM) approach and point out the hitherto unexplained features of the experiments. A detailed description of the TMM might be found in refs. [11] and [17].

The Hamiltonian for a spin-wave system driven by a microwave field is given by

$$\mathcal{H} = \mathcal{H}^{(2)} + \mathcal{H}^{(4)} + \mathcal{H}'(t), \quad (1)$$

where

$$\mathcal{H}^{(2)} = \sum_k \hbar \omega_k c_k^\dagger c_k, \quad (2)$$

is the Hamiltonian for a system of independent harmonic oscillators (magnons) with frequency  $\omega_k$ ,  $\mathcal{H}^{(4)}$  represents the four-magnon interaction and  $\mathcal{H}'(t)$  describes the interaction with the microwave field. The expectation value of the magnon operator  $\langle c_k^\dagger \rangle$  is proportional to the transverse-precessing magnetization  $m^+ = m_x + im_y$ . Since  $m^+$  gives the transverse (circularly polarized) microwave susceptibility of the sample, it is related to the amplitude-modulation signal in the subsidiary resonance experiment. In the parallel-pumping configuration, the signal is related to the *z*-component of the magnetization and thus to the magnon occupation number  $n_k = \langle c_k^\dagger c_k \rangle$ .

The nonlinear coupling of parametric magnons is provided by the four-magnon interaction, which has relevant terms of the form [7]

$$\mathcal{H}^{(4)} = \hbar \sum_{k,k'} \left( \frac{1}{2} S_{kk'} c_k^\dagger c_{-k}^\dagger c_{k'} c_{-k'} + T_{kk'} c_k^\dagger c_{k'}^\dagger c_k c_{k'} \right). \quad (3)$$

In general, exchange, dipolar and anisotropy interactions contribute to  $\mathcal{H}^{(4)}$ . For small values of  $k$  ( $\sim 10^5 \text{ cm}^{-1}$ ), such as YIG pumped by microwave fields, the contribution from the exchange energy is negligible<sup>24</sup>.

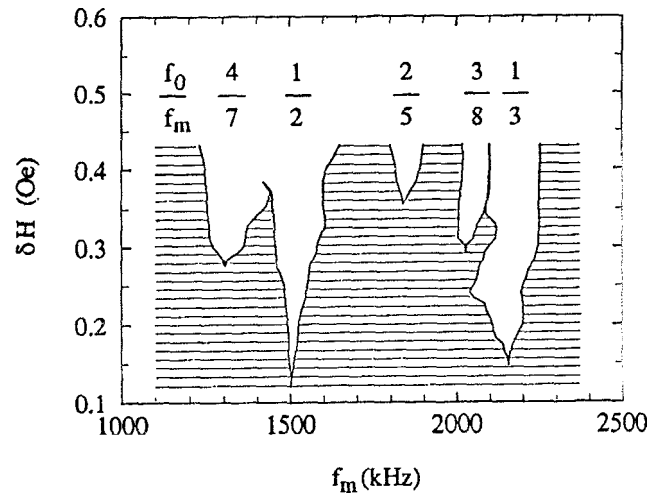


Figure 10: Critical modulation amplitude  $\delta H^*$  vs. modulation frequency  $f_m$ . The boundaries between the chaotic and controlled regions have minima at values of  $f_m$  commensurate with the fundamental frequency  $f_0$  at ratios indicated at the top [Ref.13].

We usually treat the interacting spin-wave system as if it were driven by a uniform microwave field in an infinite medium, so that  $\mathcal{H}'(t)$  preserves momentum. However, in a finite medium,  $\mathcal{H}'(t)$  can be nonzero for pairs  $\vec{k}, \vec{k}'$  for which  $k$  and  $k'$  differ by an amount of the order of the reciprocal of the sample size  $L$ . In this case, it can be shown that the driving term of the Hamiltonian becomes, either in parallel or subsidiary-

resonance pumpings,<sup>17</sup>

$$\mathcal{H}'(t) \simeq \frac{1}{2} h \sum_{k,k'} h \rho_k e^{-i\omega_p t} c_k^\dagger c_{-k}^\dagger \cdot (\delta_{kk'} + \alpha_{\Delta k} \delta_{k,k' \pm \Delta k} + \dots) + H.c., \quad (4)$$

where  $\rho_k$  expresses the coupling between the field  $h(t) = h e^{-i\omega_p t}$  and the spin wave.  $\alpha_{\Delta k}$  is a factor which depends on the wave-vector mismatch  $\Delta \vec{k} = \vec{k} - \vec{k}'$ . For instance, for two neighbouring standing waves along  $x$  with  $\Delta k_x = \pi/L_x$ ,  $\alpha_{\Delta k}$  attains its maximum value  $2/\pi \simeq 0.64$ . In an infinite medium,  $\alpha_{\Delta k} = 0$ .

The Hamiltonian (1) leads to 2N coupled nonlinear equations describing the N nearly degenerate modes excited by the pumping field. For only two modes, the equations of motion for the slowly varying spin-wave variables become<sup>17</sup>

$$\dot{c}_1 = (\gamma_1 + i\Delta\omega_1)c_1 - ih\rho_1(c_1^* + \alpha e^{i\beta/2}c_2^*) - i2(S_1c_1^2c_1^* + S_{12}c_1^*c_2^2 + 2T_{12}c_2c_2^*c_1), \quad (5)$$

$$\dot{c}_2 = (\gamma_2 + i\Delta\omega_2)c_2 - ih\rho_2(c_2^* + \alpha e^{-i\beta/2}c_1^*) - i2(S_2c_2^2c_2^* + S_{12}c_2^*c_1^2 + 2T_{12}c_1c_1^*c_2), \quad (6)$$

where  $\Delta\omega_k = \omega_k - \omega_p/2$ ,  $S_k \equiv S_{kk} + 2T_{kk}$ ,  $a \equiv \alpha_{\Delta k}$  and  $\beta \equiv \beta_{12}$  is the phase difference between modes 1 and 2.<sup>17</sup>

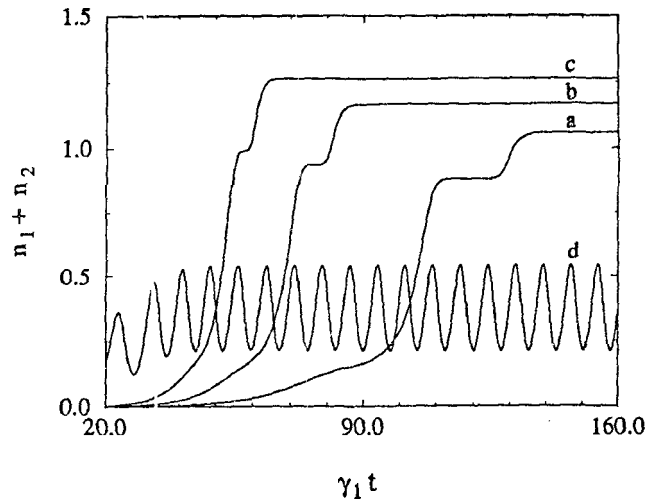


Figure 11: Numerical results of the magnon population sum  $n_1 + n_2$  obtained from eqs.(5) and (6) with  $S_1 = S_2 = -0.5$ ,  $S_{12} = 2.0$ ,  $T_{12} = -1.0$ ,  $\Delta\omega_1 = -0.2$ ,  $\Delta\omega_2 = 0.5$  and  $(\alpha, R) = (0, 1.07)$  (a),  $(0, 1.09)$  (b),  $(0, 1.11)$  (c) and  $(0.5, 1.20)$  (d). [Ref.12].

### III.1 Numerical solutions of the spin-wave equations

Equations (5) and (6) with their 12 independent parameters still represent a very complex mathematical

problem. In the numerical studies with an arbitrary set of parameters, one usually finds that the solutions are attracted to stable fixed points. In certain regions of the parameter space, some fixed points become unstable and the solutions may exhibit a variety of dynamic behavior. Due to the unclear nature of the modes involved in the dynamics, it is difficult to relate the parameters with the microscopic ones<sup>10,24</sup>.

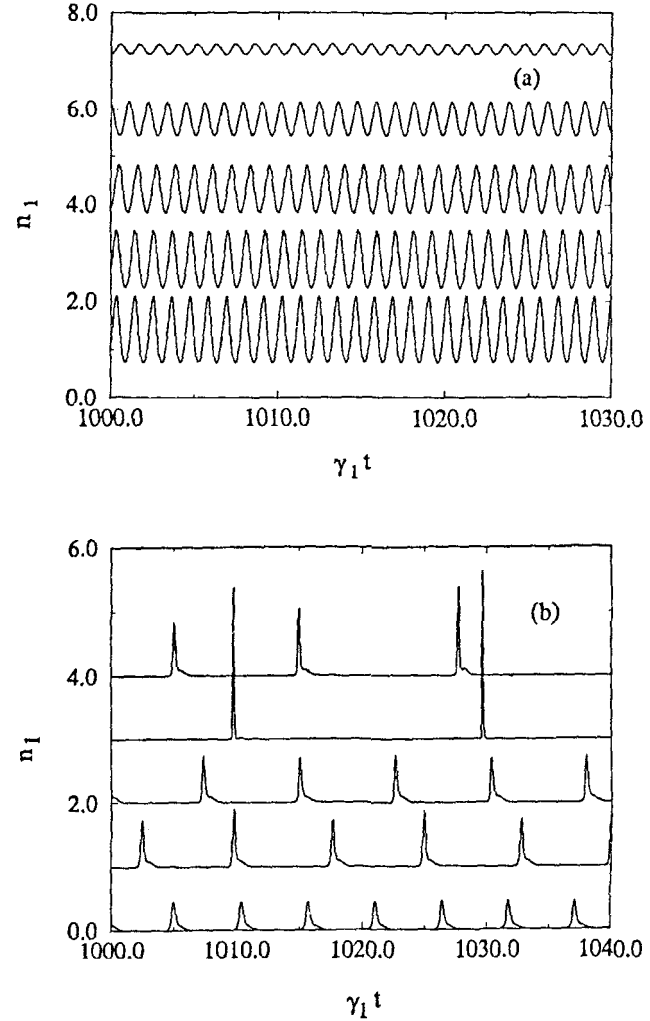


Figure 12: Numerical results for  $n_1$  vs.  $\gamma_1 t$  for two different sets of parameters in eqs.(5) and (6) (see text). (a) Hopf bifurcation and (b) homoclinic bifurcation.

Figure 11 shows the transient behavior of the normalized magnon population  $n_1 + n_2$  for several values of the pumping field  $R = h/h_c$ , for two modes described by (5) and (6) with normalized parameters  $S_1 = S_2 = -0.5$ ,  $S_{12} = 2.0$ ,  $T_{12} = -1.0$ ,  $\rho_1 = \rho_2$ ,  $\Delta\omega_1 = -0.2$  and  $\Delta\omega_2 = 0.5$ . The three step-like curves were obtained with  $\alpha = 0$  and  $R \simeq 1.07, 1.09$  and  $1.11$ . The auto-oscillation was obtained with  $R = 1.2$  but with  $a = 0.5$ . The curves showing the build-up of the first mode and subsequently the second with increasing  $R$ , have striking similarity with the experimental data of Fig.2.

Quite different behavior may occur at the onset of auto-oscillation as we can see in the experiments of Fig.4. Here we show that this can be understood as a result of particular combinations of the parameters in the TMM. Fig.12(a) shows numerical results for  $n_1$  vs.  $\gamma_1 t$  with  $\Delta\omega_1 = \Delta\omega_2 = 0$ ,  $\rho_2 = 0.7\rho_1$ ,  $\gamma_2 = 5.0\gamma_1$ ,  $S_1 = -1.0$ ,  $S_2 = 0.5$ ,  $S_{12} = 2.5$ ,  $T_{12} = 1.125$  and  $\alpha = 0$ . In this case, at  $R = R'_c \simeq 1.37$  a *Hopf bifurcation* into a limit cycle occurs, corresponding to the onset of an auto-oscillation with a finite frequency  $f_0 = 0.87\gamma_1$  and a vanishingly small amplitude. As  $R$  increases beyond  $R'_c$ , the amplitude obeys the scaling law  $A \sim (R - R'_c)^{1/2}$ , as in the experiments of Fig.4(a). Another remarkable result is shown in Fig.12(b) for  $\Delta\omega_1 = (-2\pi)0.3$ ,  $\Delta\omega_2 = (2\pi)0.2$ ,  $S_{11} = S_{22} = S_{12} = 4.078$ ,  $T_{11} = T_{22} = -1.896$ ,  $T_{12} = 0$ ,  $\rho_1 = \rho_2$ ,  $\gamma_1 = \gamma_2$  and  $\alpha = 0$  [25]. In this case, as the

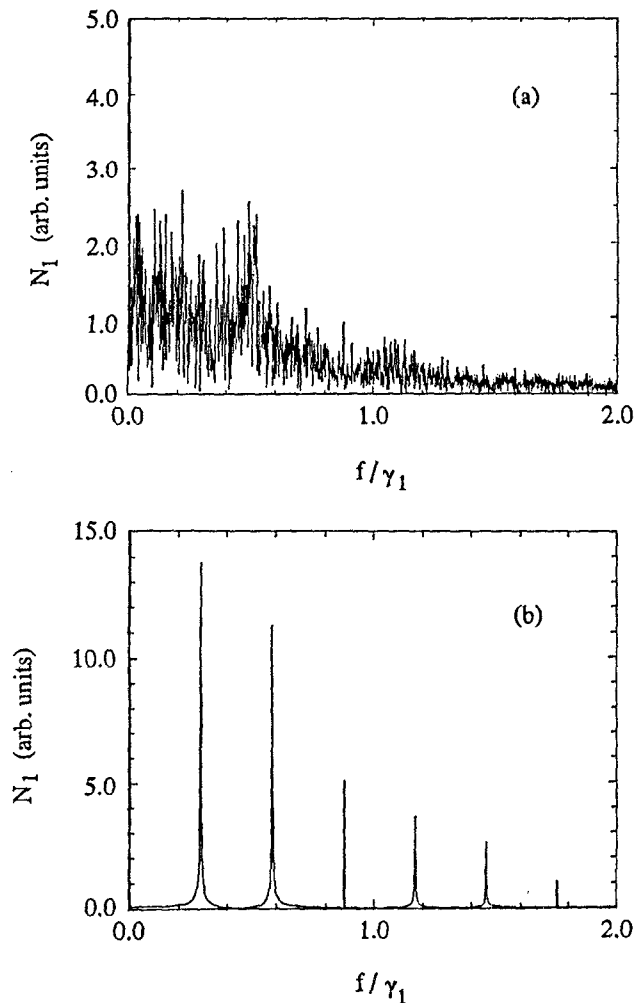


Figure 13: Power spectra of  $n_1$  for two different values of the amplitude  $\Omega$  of the modulation frequency. Parameters are given in the text. (a) Chaos for  $\Omega = 0.6$ . (b) Chaos under control with  $\Omega = 0.9$  and  $f_m/\gamma_1 = 0.875$ .

pumping field increases beyond  $R'_c \simeq 1.64$ , very-

low-frequency aperiodic spiking behavior develops in the amplitude  $n_1$ . The (average) frequency increases rapidly with  $R$ , in good qualitative agreement with the experiments of Fig.4(b). This phenomenon has been characterized as a *homoclinic bifurcation*<sup>16,17</sup>.

Subharmonic routes to chaos were extensively studied since the introduction of the TMM by Nakamura and co-workers ten years ago<sup>8,11</sup>. Here we present an additional interesting feature of this model, namely, the control of chaos. A periodic perturbation in the static magnetic field  $\delta H \cos(2\pi f_m t)$ , as the one described in the last section, corresponds to a time-dependent parameter  $\Delta\omega_k$  in the TMM,  $\Delta\omega_k \rightarrow \Delta\omega_k + \Omega \cos(2\pi f_m t)$  in Eqs.(5) and (6). In Fig.13 we show preliminary results for the power spectrum of  $n_1$  with  $R = 1.81$ ,  $\rho_1 = \rho_2$ ,  $S_1 = S_2 = 1.0$ ,  $S_{12} = -0.4$ ,  $T_{12} = -0.75$ ,  $\beta = 0$ ,  $\alpha = 0.64$ ,  $\Delta\omega_1 = \Delta\omega_2 = -1.0$ , and  $f_m/\gamma_1 = 0.875$ . Fig.13(b) shows that the chaotic state shown in Fig.13(a) for  $\Omega = 0.6$ , is under control with  $\Omega = 0.9$ , again in good qualitative agreement with the experiments (Fig.9).

### III.2 Discussion

The restriction to only two modes out of an entire degenerate manifold paved the way to a better qualitative understanding of the spin-wave nonlinear dynamics. However, the number and the nature of the excited modes still lack a definitive explanation. Considerable efforts have been focused at the onset of spin-wave auto-oscillation in the past few years. Unprecedented quantitative agreement between experiment and the microscopic theory was achieved by McMichael and Wigen<sup>26</sup>. They have used a very thin magnetic garnet film where only a few modes are excited and can be selectively tuned in the experiments. On the other hand, Suhl and Zhang<sup>27</sup> have used powerful tools of nonlinear dynamics to show that even if the entire degenerate spin-wave manifold is excited above threshold, it organizes itself into new eigenmodes of which only a few are active. Therefore, the dynamics of the system in the vicinity of the oscillation threshold is effectively governed by two modes. We regard the step transients in Fig.2 as a strong support of this idea. However, the quantitative results of Suhl and Zhang presented similar problems to those of the two-mode numerical calculations, namely, too high auto-oscillation frequency and threshold field.

Improvements in the microscopic model have recently been proposed<sup>17,28</sup>, through the inclusion of the boundary conditions in finite bulk samples. Although a better quantitative agreement for the auto-oscillation frequency and threshold field has been achieved, our model equations with  $\alpha_{\Delta k} \neq 0$  do not seem to account for all details of the experimental results, probably because they do not describe correctly the collective modes<sup>12</sup>. On the other hand, it seems to us that the build-up of discrete modes, as presented in



Fig. 2, cannot be described by the analytical approach of ref. [28]. Combined microwave and light-scattering experiments<sup>29</sup> should give important additional information on the spatial and temporal patterns in spin-wave experiments. These examples indicate that research in spin-wave nonlinear dynamics is likely to attract attention for years to come.

### Acknowledgements

We thank Prof. Jair Koiller for illuminating discussions, and Mr. Jose Americo Moura for technical assistance. This work has been supported by FIKEP, CNPq, PADCT, CAPES and FACEPE.

### References

1. N. Bloembergen and R. Damon, *Phys. Rev.* **85**, 669 (1952); N. Bloembergen and S. Wang, *ibid.* **95**, 72 (1954);
2. H. Suhl, *J. Phys. Chem. Solids* **1**, 200 (1957).
3. F. R. Morgenthaler, *J. Appl. Phys.* **31**, 95S (1960); E. Schlömann, J. J. Green and U. Milano, *ibid.* **31**, 386S (1961).
4. S. S. Hartwick, E. It. Peressini and A. T. Weiss, *J. Appl. Phys.* **33**, 223S (1961).
5. S. Wang, G. Thomas, and Ta-Lii Hsu, *J. Appl. Phys.* **39**, 2710 (1968).
6. G. Thomas and G. Komoriya, *J. Appl. Phys.* **66**, 883 (1975).
7. V. E. Zikharov, V. S. L'vov and S. S. Starobinets, *Usp. Fiz. Nauk* **114**, 609 (1974). [*Sov. Phys. Usp.* **7**, 896 (1975)].
8. K. Nakamura, S. Ohta and K. Kawasaki, *J. Phys.* **C15**, L143 (1982).
9. G. Gibson and C. Jeffries, *Phys. Rev. A* **29**, 811 (1984).
10. F. Al. de Aguiar and S. M. Rezende, *Phys. Rev. Lett.* **56**, 1070 (1986).
11. For a review, see: S. M. Rezende, A. Azevedo and F. Al. de Aguiar, *Spin-wave instabilities, auto-oscillations, chaos and control of chaos in YIG spheres*, in *Linear and Nonlinear Spin Waves in Magnetic Films and Superlattices*, edited by R. C. Cottam, World Scientific (1992) and references therein.
12. S. Al. Rezende, F. Al. de Aguiar and A. Azevedo, *J. Appl. Phys.* (to be published).
13. A. Azevedo and S. M. Rezende, *Phys. Rev. Lett.* **66**, 1342 (1991).
14. J. Giuckciiliciner and P. Holmes, *Nonlinear Oscillations, Dynamical Systems and Bifurcations of Vector Fields* (Springer, New York, 1983).
15. S. M. Rezende and F. Al. de Aguiar, *Proc. IEEE* **78**, 893 (1990); *Physica A* **163**, 232 (1990).
16. S. M. Rezende, A. Azevedo, J. Koiller and A. Cascoii, *J. Appl. Phys.* **69**, 5430 (1991).
17. S. Al. Rezende and A. Azevedo, *Phys. Rev. B* **45**, 10387 (1992).
18. F. Al. de Aguiar, Ph.D. thesis, Universidade Federal de Pernambuco (1989), unpublished; *Phys. Rev. A* **40**, 7244 (1989).
19. (a) F. Al. de Aguiar, A. Azevedo and S. Al. Rezende, *Phys. Rev. B* **30**, 9448 (1989); (b) H. Yamazaki, *J. Appl. Phys.* **64**, 5391 (1988); (c) P. F. Meier, H. R. Moser, M. Warden and F. Waldner, in *New Trends in Magnetism*, eds. A. D. Coutinho-Filho and S. Al. Rezende (World Scientific Publ., Singapore, 1990), pp231-242.
20. A. Azevedo, Ph.D. thesis, Universidade Federal de Pernambuco (1991), unpublished.
21. F. Al. de Aguiar, A. Azevedo and S. M. Rezende, *Proceedings of MMM, Houston* (1992).
22. C. Grebogi, E. Ott, F. Romeiras and J. A. Yorke, *Phys. Rev. A* **36**, 5365 (1987).
23. E. Ott, C. Grebogi and J. A. Yorke, *Phys. Rev. Lett.* **64**, 1196 (1990).
24. S. Al. Rezende, O. F. de Alcantara Bonfim and F. Al. de Aguiar, *Phys. Rev. B* **33**, 6153 (1986).
25. P. H. Bryant, C. D. Jeffries and K. Nakamura, *Phys. Rev. Lett.* **60**, 1185 (1988); *Phys. Rev. B* **38**, 4223 (1988).
26. R. D. McMichael and P. E. Wigen, *Phys. Rev. Lett.* **64**, 64 (1990).
27. H. Suhl and X.Y. Zhang, *Phys. Rev. Lett.* **57**, 1480 (1986); *Phys. Rev. B* **38**, 4893 (1988).
28. V. B. Cherepanov and A. N. Slavin, preprint.
29. S. M. Rezende and A. Azevedo, *Phys. Rev. B* **44**, 7062 (1991).